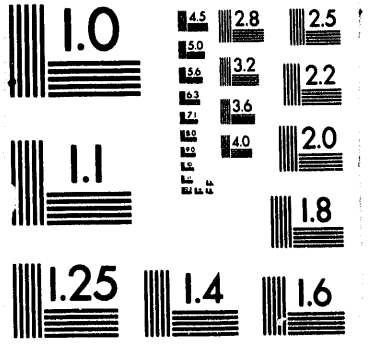
1.0
1.1
1.25
1.4
1.6
1.8
2.0
2.2
2.5
2.8
3.2
3.6
4.0
4.5
5.0
5.6
6.3
7.1
8.0
9.0

1 of 1

DOE/PC/92548--T4

Suppression of Fine Ash Formation in Pulverized Coal Flames

DOE Grant No. DE-FG22-92PC92548
Period of Performance: September 30, 1992 to January 31, 1995

Quarterly Technical Progress Report No. 4

Period Covered by Report: July 1, 1993 to September 30, 1993

Prepared by:

JOHN C. KRAMLICH
DAVID A. HOFFMAN
ERIC K. BUTCHER

Department of Mechanical Engineering, FU-10
University of Washington
Seattle, Washington 98195

Prepared for:

DOCUMENT CONTROL CENTER

U. S. Department of Energy
Pittsburgh Energy Technology Center
P. O. Box 10940, MS 921-118
Pittsburgh, Pennsylvania 15236-0940

Date Submitted: October 29, 1993

"U.S./DOE Patent Clearance is not required prior to the publication of this document."

Introduction

One of the major obstacles to the economical use of coal is managing the behavior of its mineral matter. Ash size and composition are of critical importance for a variety of reasons. Fly ash size and emissivity affect radiant furnace heat transfer.[1] Heat transfer is also affected by the tendency of ash to adhere to heat transfer surfaces,[2] and the properties of these deposits.[3] Removal of ash from flue gas by electrostatic precipitators is influenced by both particle size and particle resistivity.[4] The efficiency of fabric filter-based cleaning devices is also influenced by ash size.[5] Both types of devices have reduced collection efficiencies for smaller-sized particles, which corresponds to the size most efficiently retained in the alveolar region of the human lung.[6] This special concern for finer sized particles has led to PM10 regulations in the last several years (PM10: particles of diameter less than 10 μm).

Laboratory work and studies of full-scale coal-fired boilers have identified two general mechanisms for ash production. The vast majority of the ash is formed from mineral matter that coalesces as the char burns, yielding particles that are normally larger than 0.5 μm. Flagen and Friedlander[7] proposed a simple model for this residual ash, called the breakup model. In this model, each particle is assumed to yield its mineral matter as a certain specified number of ash particles (usually in the range of 1-5). This latter value is termed the "breakup number." In this way, a known pulverized coal size distribution can be transformed into a projected ash size distribution. The presumed mechanism is that each char particle fragments during combustion, carrying mineral matter with it. The major assumptions used in the model include: (1) all coal particles contain the same percentage of mineral matter, independently of size, (2) all coal particles break into exactly the same number of char particles during combustion, (3) each char particle contains the same amount of mineral matter as the other char particles, and (4) no further fragmentation occurs, which means that each offspring char particle yields its mineral matter as a single ash particle. The breakup number has been identified in recent work as being influenced by the breakup of the char during burnout, from shedding at the burning char surface,[8] and from the fragmentation of discrete included and excluded minerals.[9,10] Recent experimental work[11] and elegant site percolation modeling[12] indicate that char macroporosity is the single most important factor governing char breakup and residual ash size. Despite the severity of the assumptions, the basic breakup model has proven to be a useful engineering and interpretative tool.[13]

The second major mechanism is the generation of a submicron aerosol through a vaporization/condensation mechanism. When the ash size distribution is plotted in terms of number density, the submicron mode generally peaks at about 0.1 μm.[4] When plotted in terms of mass, this mode is sometimes distinct from the residual ash mode,[13] and sometimes merged into it.[14] During diffusion-limited char combustion, the interior of the particle becomes hot and fuel-rich. The non-volatile oxides (*e.g.*, Al_2O_3, SiO_2, MgO, CaO, Fe_2O_3) can be reduced to more volatile suboxides and elements, and partially vaporized.[15-17] These reoxidize while passing through the boundary layer surrounding the char particle, thus becoming so highly supersaturated that rapid homogeneous nucleation occurs. This high nuclei concentration in the boundary layer promotes more extensive coagulation than would occur if the nuclei were uniformly distributed across the flow field.[18] The vaporization can be accelerated by the overshoot of the char temperature beyond the local gas temperature.[19]

Although these particles represent a relatively small fraction of the mass, they can present a large fraction of the surface area. Thus, they are a preferred site for the condensation of the more volatile oxides later in the furnace. This leads to a layering effect in which the refractory oxides are concentrated at the particle core and the more volatile oxides reside at the surface.[20] This also explains the enrichment of the aerosol by volatile oxides that has been noted in samples from practical furnaces.[21] These volatile metal oxides include the majority of the toxic metal contaminants, *e.g.*, mercury, arsenic, selenium and nickel. Risk assessment studies suggest that toxic metal emissions represent a significant portion of the health risk associated with combustion

systems.[22]

Previous work has shown that pulverized bituminous coals that were treated by coal cleaning (via froth flotation) or aerodynamic sizing exhibited altered aerosol emission characteristics. Specifically, the emissions of aerosol for the cleaned and sized coals increased by as much as one order of magnitude. At least three mechanisms have been proposed to account for this behavior.

Objectives

The goals of the present program are to:

1. Perform measurements on carefully characterized coals to identify the means by which the coal treatment increases aerosol yields.

2. Investigate means by which coal cleaning can be done in a way that will not increase aerosol yields.

3. Identify whether this mechanism can be used to reduce aerosol yields from systems burning straight coal.

Progress - Mechanistic Interpretation

One of the weaknesses of our earlier work on cleaned coals was the exclusive use of coals that were relatively high in sodium.[23,24] The Utah coal is typical of western bituminous coals in that it is high in sodium. The Illinois No.6 is also high in sodium, especially compared with other eastern bituminous coals. This problem has been addressed in coal selection for the present work, as described in the next section.

Some of the mechanisms associated with sodium release from coal char combustion have been addressed in the recent work by Gallagher[25] and the review by Linak and Wendt.[26] These works suggest that sodium release is a complex process in which the fundamental vaporization mechanism competes with sodium capture by aluminosilicate mineral inclusions. Once captured, the sodium becomes complexed and either cannot be again released, or its release is delayed to much higher temperatures. Thus, the amount of sodium that is released as vapor to form aerosol is strongly dependent on the quantity and dispersion of the aluminosilicate inclusions.

This picture of the sodium vaporization process suggests additional interpretations on our earlier data. Since the sodium content within the mineral matter was relatively high for these coals, one hypothesis is that the bulk of our aerosol originated as sodium vapor. In the untreated coals (*i.e.*, before the froth floatation cleaning step) the coals may contain loosely attached aluminosilicate mineral matter on the surface of the macerals. These could act as sinks for sodium vapor. In addition, aluminosilicate inclusions within the char particle could also act as sinks for sodium vapor. In fact, if enough inclusions are present within the particle, the amount of sodium vapor reaching the surface could be significantly reduced.

To provide a preliminary evaluation of these possibilities, a simple model has been formulated. This model will also serve as a basis for further model development and further interpretation of data developed during this project. This will be described in the following paragraphs.

Model Description

The model assumes a spherical char particle burning in a diffusion-limited mode. This means that the interior of the particle is under a reducing environment. Sodium is assumed to be organically

bound, *i.e.*, bound to carboxyl groups. Due to the molecular dispersion of the sodium throughout the char, there is essentially no resistance to the sodium entering the vapor phase. Thus, at any point in the char the partial pressure of the sodium is equal to the equilibrium pressure over the bound sodium at the local temperature. This holds at all points where sodium remains in the solid phase, but not where the sodium has become depleted.

Before including aluminosilicates in the model, we will discuss the implications of the assumptions listed above on sodium release behavior. This is illustrated in the following simplified example. Consider a spherical char particle that contains no mineral matter except molecularly dispersed sodium. As illustrated in Figure 1, initially sodium is present throughout the particle at its equilibrium partial pressure. Since the partial pressure of sodium at the surface of the particle is also at the equilibrium value, the vaporization rate will be governed by the diffusion film resistance between the surface of the particle and the free stream. This situation will hold only momentarily, however. Due to vaporization, the bound sodium in the shell near the surface will become depleted and the sodium will have to diffuse from within the particle to reach the surface, as is also shown in Figure 1. Thus, in general, the vaporization rate will be governed by the combination of the diffusion resistance in the char and the external film resistance. The depletion of sodium with time is represented by a shrinking core within which the equilibrium partial pressure of sodium is maintained. The diffusion can be considered to be fast compared to the rate of core shrinkage, so the problem can be treated as a quasi-steady-state solution. The instantaneous vaporization rate can then be evaluated as the rate at which sodium vapor arrives at the surface of the char particle.

As noted in the literature, this simplified picture must be modified to account for the absorption of sodium by aluminosilicates to form complexes. Once absorbed into these complexes, the sodium release will be delayed, if it occurs at all. These complexes will typically occur in two forms: (1) as discrete inclusions scattered within the char particle, and (2) as excluded mineral matter loosely attached to the char surface. In the work of Quann and Sarofim on the vaporization of refractory oxides, the inclusions were regarded as sources of refractory mineral vapor.[17] Here they are regarded as sinks for sodium.

To accommodate this the model for sodium release described above is modified in the following two ways:

1. Aluminosilicate inclusions are assumed to be dispersed within the char matrix. Although their effect is local, the large number and uniform dispersion of these particles allows them to treated mathematically as a continuum sink of finite strength dispersed throughout the char. These will be active in both the shell region and in the equilibrium core illustrated in Figure 1.

2. Aluminosilicate particles at the edge of the char particle. These can act as sinks for sodium leaving the char particle. These can be handled mathematically by a modification of the boundary conditions at the char surface.

The next section discusses the mathematical formalism.

Model Formulation

For consistency, we have adopted as much of the nomenclature of Quann and Sarofim as possible.[17] We first write and solve a conservation equation for sodium vapor within the shell region shown in Figure 1. Here the transport of sodium vapor is governed by the following equation:

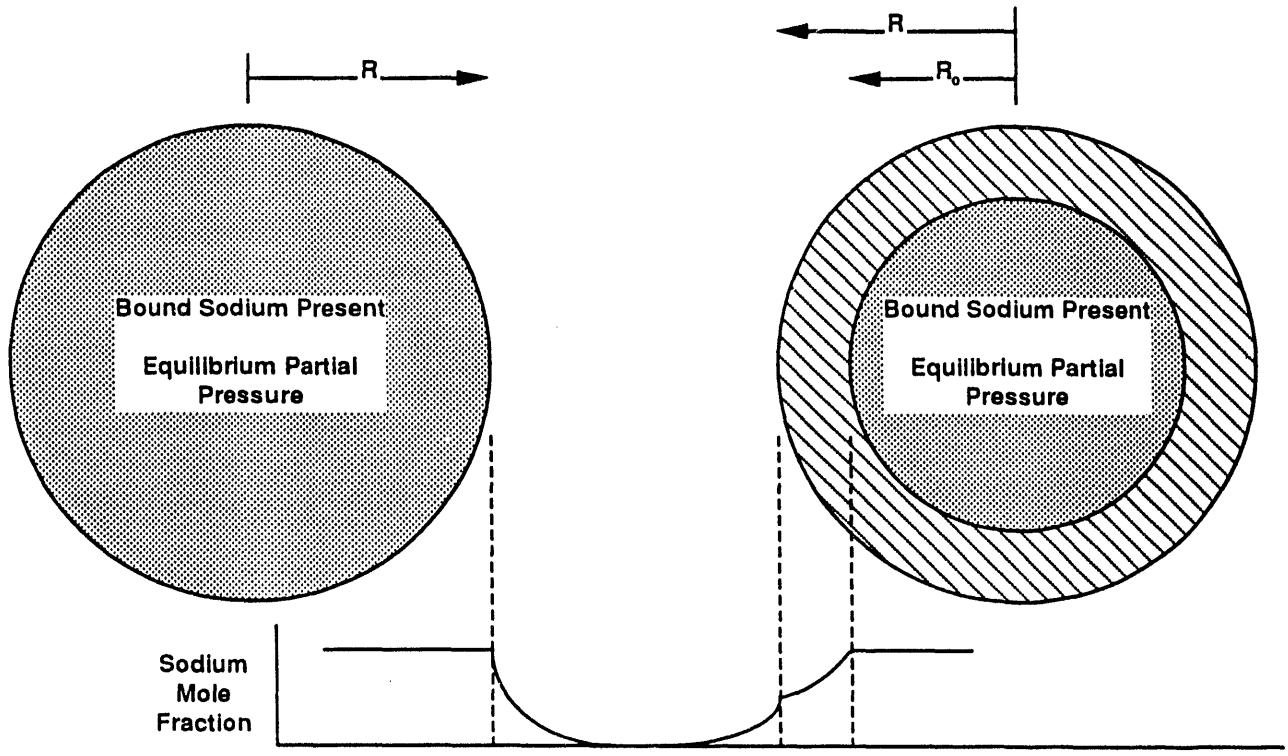

Char particle at start of sodium vaporization. The partial pressure is uniform, and the surface concentration of the sodium is also at the equilibrium value. Vaporization rate is governed by diffusion through the external gas film

Char particle partway into vaporization. Within core partial pressure remains uniform, but within shell the bound sodium is depleted. Vaporization rate is governed by Knudsen diffusion through shell and diffusion through the external gas film

Figure 1. Schematic of char particles showing sodium vapor profiles for two stages in the vaporization lifetime.

$$cD_e \frac{1}{r^2} \frac{d}{dr}\left[r^2 \frac{dy_{Na}}{dr}\right] - \rho_{Na} V_{Na} = 0 \qquad (1)$$

where: c = molar density of total gas (kmoles/m^3)
D_e = Knudsen coefficient for diffusion of Na vapor in the porous char (m^2/s)
y_{Na} = mole fraction of Na in vapor
ρ_{Na} = number density of aluminosilicate inclusions (m^{-3})
V_{Na} = rate of absorption of Na by a single inclusion (kmoles/s)

If the mole fraction of sodium vapor at the surface of the inclusions is zero, then the rate of sodium transport to the inclusions will be governed by the rate of diffusion of sodium from the bulk of the char to the surface of the inclusions. This is calculated by integrating the diffusion equation around each inclusion. Assuming no local convective velocity, the transport rate is:

$$V_{Na} = 4\pi R_i c D_e y_{Na} \qquad (2)$$

where R_i is the radius of the inclusion, and y_{Na} is the mole fraction of sodium in the "free stream" vicinity near the inclusion.

Equation 1 can be transformed by the substitution $y_{Na} = f/r$ into the following form:

$$\frac{d^2 f}{dr^2} - \lambda^2 f = 0 \qquad (3)$$

where: $\lambda^2 = 4\pi R_i \rho_{Na}$

This has solutions: $f(r) = A \exp(\lambda r) + B \exp(-\lambda r)$, or

$$y_{Na}(r) = \frac{A R_O}{r} \exp(\lambda r) + \frac{B R_O}{r} \exp(-\lambda r) \qquad (4)$$

where A and B are constants. At the inner boundary the mole fraction of sodium is at the local equilibrium value:

$$\text{at } r = R_o, \; y_{Na} = y_{Na,e} \qquad (5)$$

The outside boundary has a hybrid boundary condition. In the absence of mineral matter on the surface, a convective external boundary condition will prevail:

$$\frac{dy_{Na}}{dr} + \frac{D_O \alpha}{R c D_e} y_{Na} = 0 \qquad \text{all at } r=R \qquad (6a)$$

here, the gradient is on the char side of the surface, D_O is the ordinary diffusivity and α is a correction term for Stefan flow, as outlined in Quann and Sarofim.[17] If the surface is entirely coated with aluminosilicate particles, then the surface concentration of sodium is zero, as expressed by:

$$\text{at } r=R, \; y_{Na}=0 \qquad (6b)$$

The assumption is made that the surface mineral matter is sufficiently well dispersed to act in a "finely speckled" absorber of sodium vapor. Here, the radial symmetry of the sodium vapor profile within the char particle is not disturbed, but both the surface concentration and the vapor flux leaving the char are influenced by the fraction of the surface that is covered by minerals. This situation is approximated by considering the actual solution for the sodium vapor profile within the char to be a linear combination of the following two solutions:

1. $y_{Na,1}$ = solution subject to boundary condition (6a).

2. $y_{Na,2}$ = solution subject to boundary condition (6b).

so the final solution is: $y_{Na}(r) = (1-\varepsilon)\, y_{Na,1} + \varepsilon\, y_{Na,2}$, where ε is the fraction of the char surface that is covered by minerals that act as sinks for sodium vapor.

These individual solutions require substantial algebraic manipulation, but are straightforward, and are given in final form here:

$$y_{Na,1} = \frac{R_O\, y_{Na,e}}{r} \left\{ \left[1 - \frac{1}{1 + \frac{\lambda - M}{\lambda + M} \exp(-2\lambda R) \exp(-2\lambda R_O)} \right] \frac{\exp(\lambda r)}{\exp(\lambda R_O)} \right\} + \left[\frac{1}{1 + \frac{\lambda - M}{\lambda + M} \exp(-2\lambda R) \exp(-2\lambda R_O)} \right] \frac{\exp(-\lambda r)}{\exp(-\lambda R_O)} \tag{7}$$

here, $$M = \frac{1}{R}\left[\frac{D_O \alpha}{c\, D_e} - 1\right]$$

and:

$$y_{Na,2} = \frac{R_O}{r}\left[\frac{\exp(\lambda R_O)}{1 - \exp(2\lambda R_O - 2\lambda R)}\right]\left[\exp(-\lambda r) - \exp(-2\lambda R)\exp(\lambda r)\right] \tag{8}$$

From this solution, the instantaneous vaporization rate of sodium can be established. The rate at which sodium arrives at the surface from within the char is given as:

$$\text{Rate} = -4\pi R^2\, c\, D_e \frac{dy_{Na}}{dr} \tag{9}$$

Of the vapor arriving at the surface, only the fraction $(1 - \varepsilon)$ escapes, the remaining fraction being captured by the surface minerals. Thus, the final expression for the rate of escape of sodium vapor away from the particle is given by:

$$\text{Vaporization Rate} = 4\pi R^2 (1-\varepsilon)\, c\, D_e \frac{dy_{Na}}{dr} \tag{10}$$

or in terms of the surface concentration (char side):

$$\text{Vaporization Rate} = 4\pi R (1-\varepsilon) c D_O \propto y_{Na,s} \qquad (11)$$

This completes the quasi-steady solution for sodium transport out of the particle.

The Unreacted Core

One additional conservation equation is needed for the bound sodium within the "unreacted" core. In this core, the vapor phase concentration of the sodium is at the local equilibrium value. Locally, however, the aluminosilicate inclusions will continue to absorb sodium out of the vapor phase, as outlined above. This will be replenished by the organically-bound sodium. Thus, as time progresses, the concentration of bound sodium within the core will decrease, even though there is no diffusion of sodium to the boundary of the core. The rate at which the boundary of the core recedes is then set to match the flux of sodium entering the shell where $r>R_O$.

Within the unreacted core, the mass fraction of sodium in the char (x_{Na}) will be governed by the following equation:

$$\frac{dx_{Na}}{dt} = \frac{\rho_I}{\rho_c}\frac{1}{M_{Na}} R_i c D_e y_{Na,e} \qquad (12)$$

where ρ_c = char bulk density (kg/m^3), and M_{Na} = molar mass of Na (kg/kmole). The surface of the unreacted core must recede at a rate which supplies the correct amount of sodium to the shell layer. Thus, the rate at which the surface recedes is set by a sodium flux balance:

$$\frac{dR_O}{dt} = \frac{M_{Na} c D_e}{x_{Na}\rho_c}\left[\frac{dy_{Na}}{dr}\right] \qquad (13)$$

where dy_{Na}/dr is evaluated from the shell at the inner surface. Note that as the bound sodium is depleted, the shrinking rate of the core will increase to provide the needed sodium for shell. Also note the core may have one of two fates:

1. The core shrinks to $R_O = 0$.
2. At some point, the bound sodium within the core becomes fully consumed by the aluminosilicate inclusions, and the core vanishes homogeneously.

The specific conditions will determine the mode of core disappearance.

Current Status

This initial model is currently being coded, and the physical parameters are being entered. Initial attention is being focused on the Illinois No. 6 coal because (1) it is relatively high in sodium for an eastern bituminous coal, (2) it was used in our earlier program, and (3) detailed mineral characterization analyses are available on this coal from the PSI program.

Progress - Furnace Modification

The bulk of the work during the present quarter has been associated with furnace modification. The following section provides a brief overview of the furnace design. This is followed by a discussion of the specific progress during this quarter.

Furnace Design Goals

The fundamental goal of the furnace design is to provide a sufficient temperature and residence time to ensure complete coal burnout. Based on past experience with similar types of experimental furnaces, a main burner firing rate of 16.1 kW (55,000 Btu/hr) was chosen. Additionally, in order to ensure burnout, the furnace stoichiometry was set to provide 7% free oxygen after combustion.

Figure 1 shows a sketch of the furnace as it will look after installation. The unit will have natural gas, air, and cooling water brought into the appropriate accessories. The main burner sits atop the furnace, and the four back-fired burners, forming two pairs of heating channels, can be seen in the middle section of the furnace. Figure 2 is a cross-section of the furnace showing the multiple refractory layer design. The inner tunnel diameter is 20.3 cm (8 inches) and the overall outside diameter is 91.5 cm (36 inches). This requires 35.5 cm (14 inches) thickness of insulating material. In spite of this relatively thick layer of insulation, heat transfer calculations show that the combustion gas temperature may drop by up to 200°C as the gases move down the tunnel and reach the exhaust piping. Thus, the two pairs of backfire burners were included. These are designed to be operated independently to provide whatever inner tunnel temperature profile is desired. Each of the four back-fired burners can operate at up to 16.1 kW, but will likely run at a lower firing rate. The maximum flame temperature will be 1600°C, and this can be varied by controlling the burner air flow rate.

Furnace Construction

During this quarter, all portions of the furnace were completed, with the exception of:

- The exhaust ducting, which is being fabricated out of stainless steel in the university shops.
- The flame safety system, which is approximately 90% installed.

The use of an alternate impactor has been arranged with the Civil Engineering department. This is the Mark V, University of Washington impactor system, which will provide more size resolution in the submicron range than the Anderson impactor used previously.

Coal Selection

Following review of the PSI coal analyses, the following coals were selected for testing. One drum of each has been received, with the exception of the Beulah coal, where restricted supplies at PSI limited the shipment to a single small container.

- Upper Freeport: This is a reduced sodium coal. It contains coarse pyrite particles that are readily washed from the coal.

- Kentucky No. 11: Also low in sodium. Contains fine pyrite particles, and is not easily beneficiated.

- Illinois No. 6: Used in previous program. Relatively high in sodium, primarily as feldspar. Many fine pyrite particles.

- Beulah Lignite: Used in previous program. Contains very high organically bound Na, so it is a good candidate for blending to test sodium vapor capture hypotheses.

References

1. Gupta, R. J. *Radiative Transfer Due to Fly Ash in Coal Fired Furnaces*, Ph.D. Dissertation

1983, University of Newcastle.
2. Walsh, P. M., Sayre, A. N., Loehden, D. O., Monroe, L. S., Beér, J. M., and Sarofim, A. F. *Prog. Energy Combust. Sci.* 1990, **16,** 327.
3. Field, M. A., Gill, D. W., Morgan, B. B., and Hawksley, P. G. W. *Combustion of Pulverized Coal.* 1967, The British Coal Utilization Research Association.
4. McCain, J. D., Gooch J. P., and Smith, W. B. *Journal of the Air Pollution Control Association* 1975, **25,** 117.
5. Friedlander, S. K. *Smoke, Dust and Haze* 1977, Wiley.
6. Morrow, P. E. *Amer. Ind. Hyg. Assoc. J.* 1964, **25,** 213.
7. Flagen, R. C., and Friedlander, S. K. *Recent Developments in Aerosol Science.* (D. T. Shaw, Ed.) 1978, Wiley, Chapter 2.
8. Helble, J. J., and Sarofim, A. F. *Combust. Flame* 1989, **76,** 183.
9. Baxter, L. L. *Prog. Energy Combust. Sci.* 1990, **16,** 261.
10. Srinivasachar, S., Helble, J. J., and Boni, A. A. *Prog. Energy Combust. Sci.* 1990, **16,** 281.
11 Helble, J. J., and Sarofim, A. F. *Combust. Flame* 1989, **76,** 183.
12. Kang, S., Helble J. J., Sarofim A. F., and Beér, J. M. *Twenty-Second Symposium (International) on Combustion* 1988, The Combustion Institute, p. 231.
13. Flagen, R. C. *Seventeenth Symposium (International) on Combustion* 1979, The Combustion Institute, p. 97.
14. Linak, W. P., and Peterson, T. W. *Aerosol Sci. Technol.* 1984, **3,** 77.
15. Neville, M., Quann, R. J., Haynes, B. S., and Sarofim, A. F. *Eighteenth Symposium (International) on Combustion,* 1981, The Combustion Institute, p. 1267.
16. Senior, C. L., and Flagen, R. C. *Aerosol. Sci. Technol.* 1982, **1,** 371.
17. Quann, R. J., and Sarofim, A. F. *Nineteenth Symposium (International) on Combustion* 1982, The Combustion Institute, p. 1429.
18. Damle, A. S., Ensor, D. S., and Ranade, M. B. *Aerosol Sci. Technol.* 1982, **1,** 119.
19. Quann, R., Neville, J. M., and Sarofim A. F. *Combust. Sci. Technol.* 1990, **74,** 245.
20. Gladney, E. S., Small, J. A., Gordon, G. E., and Zoller, W. H. *Atmos. Environ.* 1976, **10,** 1071.
21. Linak, W. P., and Peterson, T. W. *Twenty-First Symposium (International) on Combustion* 1986, The Combustion Institute, p. 399.
22. Smith, A. H., and Goeden, H. M. *Combust. Sci. Technol.* 1990, **74,** 51.
23. Kramlich, J. C., and Newton, G. H., Influence of coal properties and pretreatment on ash aerosol yield. *Fuel,* in press (1993).
24. Kramlich, J. C., and Newton, G. H., Influence of coal rank and pretreatment on residual ash particle size. *Fuel Proc. Technol.,* in press (1993).
25. Gallagher, N. B. Alkali metal partitioning in a pulverized coal combustion environment. Ph.D. Dissertation, Department of Chemical Engineering, University of Arizona, Tucson, AZ (1992).
26. Linak, W. P., and Wendt, J. O. L. *Prog. Energy Combust. Sci.* **19,** 145 (1993).

DATE
FILMED
2/15/94
END